To curl or not to curl : wind tunnel investigation of spinnaker performance

Nicolas Aubin, Benoit Augier, Julien Deparday, Matthieu Sacher

TO CURL OR NOT TO CURL: WIND TUNNEL INVESTIGATIONS OF SPINNAKER PERFORMANCE

N. Aubin, Naval Academy Research Institute, France, nicolas.research.aubin@gmail.com
B. Augier, Naval Academy Research Institute, France, benoit.augier@ecole-navale.fr
J. Deparday, Naval Academy Research Institute, France, julien.deparday@gmail.com
M. Sacher, Naval Academy Research Institute, France, matthieu.sacher@ecole-navale.fr

This work presents a wind tunnel experimental study of the effect of curling on the spinnaker aerodynamic performance. Four spinnakers combining two different panellings and sail materials are tested at different wind speeds and wind angles in the Twisted Flow Wind Tunnel of the University of Auckland. Results show that the curling has a significant benefit on the propulsive force at an AWA $\geq 100°$ when this conclusion cannot be made at lower AWA where the best propulsive force is reached on the verge of curling or before. Sail material and panelling have an effect on the sheet length where curling appears, stiffer material and cross cut panelling being the latest to curl. Finally, it is shown that the curling frequency increased linearly with the flow speed at AWA $= 120°$.

NOMENCLATURE

Symbol	Definition	(unit)
f_c	Natural curling frequency	(Hz)
f_{rc}	Reduced natural curling frequency	$(-)$
C_{F_x}	Drive force coefficient	$(-)$
C_{F_y}	Side force coefficient	$(-)$
$C_{F_{sheet}}$	Sheet load coefficient	$(-)$
F_i	Drive x, side y force	(N)
L_{sheet}	Sheet length	(mm)
q	Dynamic pressure $q = \overline{\frac{1}{2}\rho U^2_{Pitot}}$	(Pa)
S	Sail area	(m^2)
U_{Pitot}	Reference wind speed	$m.s^{-1}$
β_{AW}	Apparent wind angle	(°)
ρ	Density of air	($kg.m^{-3}$)

AWA	Apparent Wind Angle

1 INTRODUCTION

To achieve efficient downwind performance, sailors usually trim downwind sails on the verge of curling. The curling of the luff is indeed a good visual indicator for the assumed most efficient trim. At a specific fixed length of the clew sheet, the luff starts to naturally fold and unfold periodically. Nevertheless curling (also known as flapping) has only been recently scientifically studied thanks to full-scale experiments ([14, 13, 7]). It has been shown that this phenomenon is a complex three-dimensional Fluid-Structure Interaction. A high suction of pressure appears near the folding area during the unfolding stage producing a temporary significant increase of the aerodynamic load. The curling is however associated to a small decrease of the aerodynamic load when the luff starts folding. Due to the non-controlled environment conditions, it has not been possible to ascertain from these full-scale experiments if the sail trim is more efficient when the luff is curling than when the sail is slightly trimmed in.

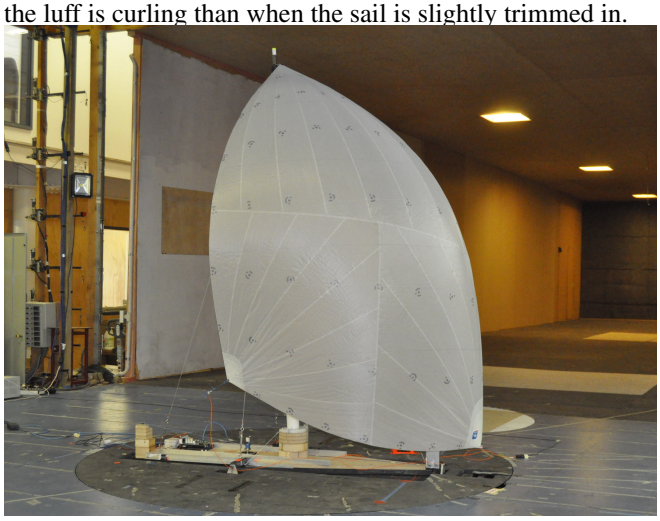

Figure 1: Triradial spinnaker tested

To better assess the aerodynamic performance of downwind sail, [19] has numerically provided insights into the flow behaviour, in particular in the luff area. Numerical simulations in [20] have also been performed on a fixed sail shape validated with wind tunnel experiments on flexible ([21, 22, 23]) and semi-rigid sails ([4, 5]). Recent projects focused on the leading edge vortex flow pattern observed on downwind sail shape show promising results in the possible use of this phenomenon in other applications ([1, 24]).

Nonetheless, the realistic fluid-structure interaction simulations of downwind sails represent a significant step forward. The step is in considering the great influence of the added mass and simulating the curling of the luff which is challenging mostly due to very large deformations of

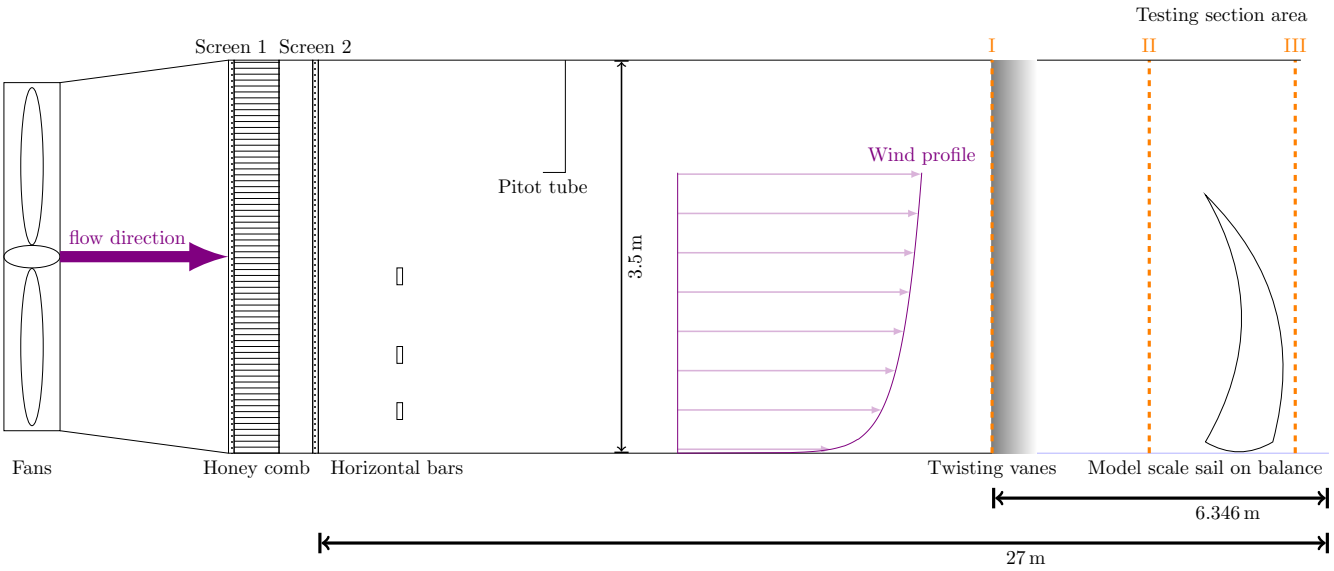

Figure 2: Twisted Flow Wind Tunnel, the University of Auckland

the sail, requiring specific and complex mesh deformation methods. As a first approach, a finite element method has been coupled to a fluid solver [16, 18] in order to predict the sail flying shape in static simulations. Results could be compared to wind tunnel validation cases like [17]. [12] and [8, 9, 10] successfully achieved unsteady fluid-structure interaction simulations, but so far such simulations have not been compared to full-scale or wind tunnel experimental unsteady data, such as the dynamic curling behaviour at a fixed trim.

Unlike the full-scale tests, wind tunnel experiments are conducted in a controlled environment ([11]). Loads are usually measured onto the boat frame ([21, 6]) and flying shape reconstruction is facilitated by the dry and large workplace. In wind tunnel, downwind sails tests are performed at a fixed "optimal trim". It is usually defined as the trim configuration where the propulsive force is maximal and when the sail shape is quasi-steady in time, i.e. when there is no curling of the luff. Hence, according to the authors' knowledge, no study has ever been published to show the effect of curling occurrence on the evolution of downwind sail performance according to the sail trim from overtrimmed to overeased. The present article provides information on the dynamic effect of curling on a spinnaker through its full range of trim.

This paper presents a wind tunnel experimental study on the effect of the curling occurrence on the aerodynamic performance of a spinnaker as shown in Fig. 1. Flying shapes, propulsive force, side force and sheet load are measured for a wide range of trim settings, from largely overtrimmed sail (spinnaker not curling) to completely eased out (spinnaker curled with a permanent fold). The influence of the sail panelling and materials is also presented. This large range of wind speed, wind angle and trim settings dynamically measured would therefore contribute to build a rich database for unsteady numerical/experimental comparisons.

The experimental set-up and the sails used for this study are firstly described. Then the results for the different sails and conditions tested are presented and highlight the effect of the occurrence of curling on the sail performance. Eventually specific dynamic aspects of the curling phenomenon are characterised in the last section.

2 EXPERIMENTAL APPARATUS

2.1 WIND TUNNEL

The experimental campaign was carried out in 2016 in the Twisted Flow Wind Tunnel ([11]) of the University of Auckland, New Zealand illustrated in Fig. 2, thanks to the Sailing Fluids collaboration program. The model was set up onto a balance (described in [2]) which can measure the different aerodynamic forces. The open jet testing section is 7 meter wide by 3.5 meter high. This paper focuses onto the drive force F_x (aligned with the boat centreline), the side force F_y (perpendicular to the boat centreline) and the sheet load F_{sheet} provided by a load sensor attached to the clew point of the spinnaker. An upstream Pitot tube measured the reference wind speed U_{Pitot} providing the averaged reference dynamic pressure q used to define the dynamic force coefficient $C_{F_i}(t) = \frac{F_i(t)}{qS}$ where i stands for x, y or $sheet$ forces. The dynamic results are averaged over 30 s long runs at a sampling frequency of 200 Hz to define the coefficient mean value:

$$C_{F_i} = \overline{C_{F_i}(t)} = \frac{\overline{F_i(t)}}{qS} \quad (1)$$

A remote control stepper motor was used to control the sheet length. In the presented cases, the sheet length was kept constant during each run. The 20 mm diameter carbon fibre mast was cantilevered and fully rigged. The twisting vanes were not used during the experimental campaign to facilitate future numerical comparisons. Four HD triggered cameras were used to record the flying shape of the sail on which 54

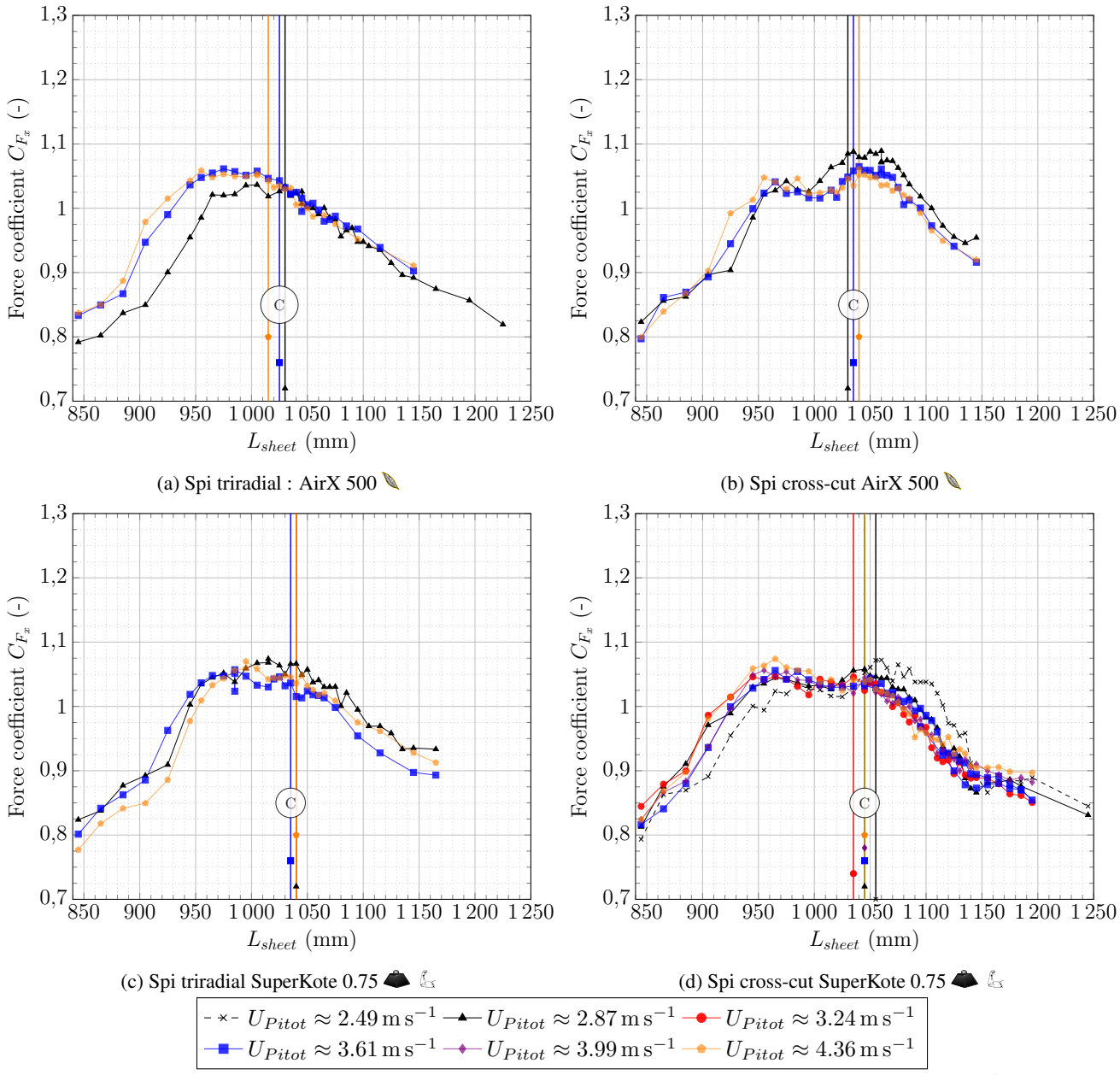

Figure 3: Drive force coefficient C_{F_x} at $\beta_{AW} = 80°$ for 4 different spinnakers. Vertical lines associated to Ⓒ represent the verge of curling for each flow velocity tested.

coded targets had been taped for photogrammetry post processing and flying shape reconstruction.

2.2 SPINNAKER PRESENTATION

Four 1:4.6 model scale J80 spinnakers with identical design shape and an area $S = 3.187\,\mathrm{m}^2$ were designed and manufactured by Incidence Sails (see Fig. 8). The differences between the spinnakers are about the material and the panelling. Two materials are used: either the AirX 500, which is the lighter material of the study illustrated by the symbol or the SuperKote 0.75 materials, heavier but also 40% stiffer, illustrated by the symbols . Two panelling type are used: a triradial one illustrated in Fig. 8a or a cross-cut one as illustrated in Fig. 8b.

3 WIND TUNNEL RESULTS

The effect of occurence of curling on the drive force is presented first at three different AWA from 80° to 120° for the four spinnakers. The effect of curling on side force and sheet load is then presented for a representative case.

3.1 EFFECT OF APPARENT WIND ANGLES AND FLOW SPEED

The influence of the apparent wind angle and speed is presented here. Three different apparent wind angles ($\beta_{AW} = 80°$; $\beta_{AW} = 100°$; $\beta_{AW} = 120°$) are tested with different flow speed velocities from $2.49\,\mathrm{m.s^{-1}}$ to $4.36\,\mathrm{m.s^{-1}}$. The evolution of the force coefficient is plotted for the different

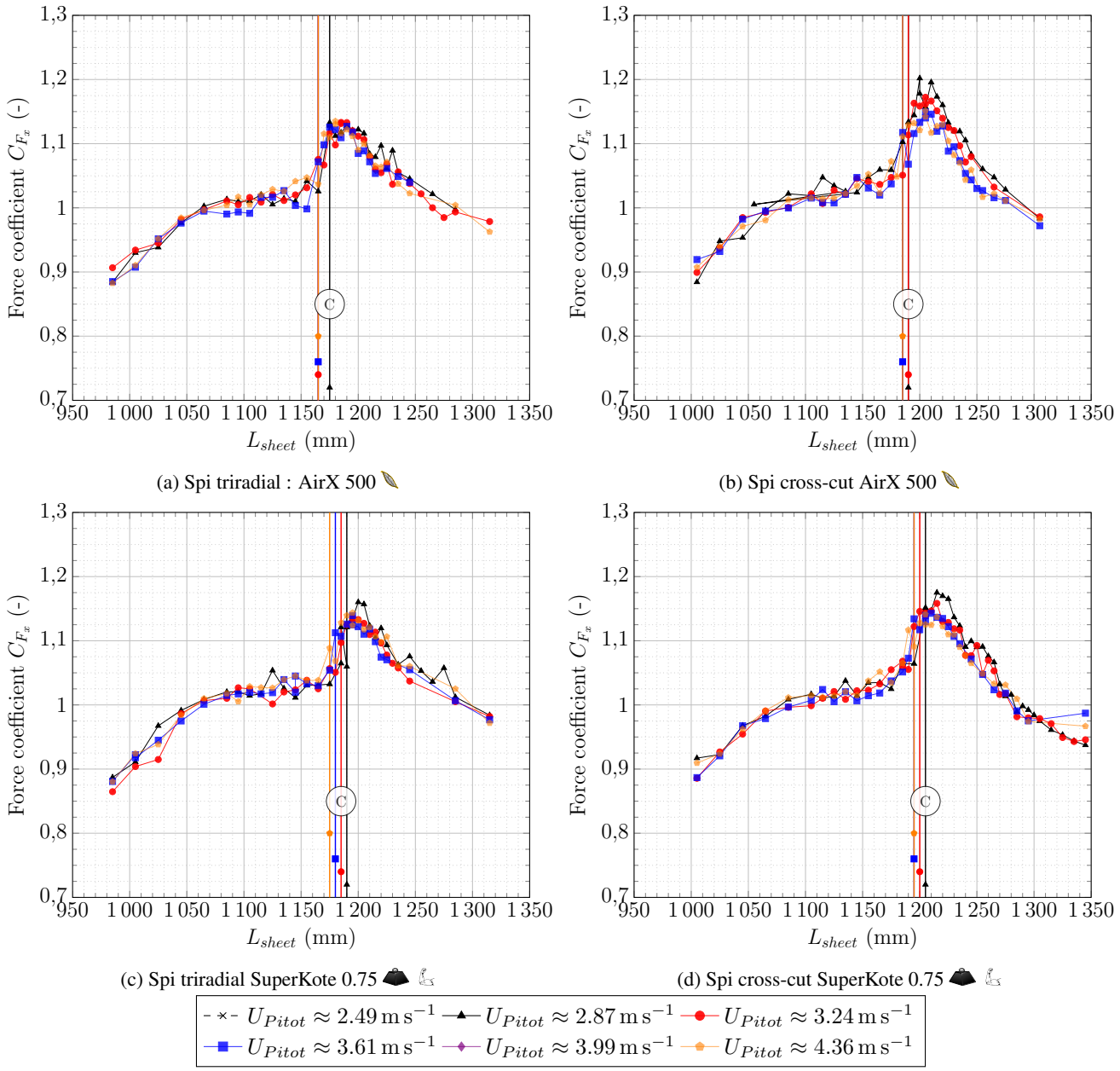

Figure 4: Drive force coefficient C_{F_x} at $\beta_{AW} = 100°$ for 4 different spinnakers. Vertical lines associated to Ⓒ represent the verge of curling for each flow velocity tested.

static sheet lengths tested. For each run serie -i.e. combination of a spinnaker, a wind speed, and an AWA for different sheet length- the test starts from an overtrimmed state, corresponding to the low sheet length value and ends with an overeased state, with greater sheet length (left to right on Figs. 3, 4, 5). The sheet is eased until luff curling appears which is represented by a vertical line with the symbol Ⓒ on the graphs. This vertical limit is associated to the state defined by sailors as "the verge of curling". Then, as the sheet length increases, curling continues until the sail reaches an overeased state where the flapping is replaced by a permanent fold.

3.1.1 $\beta_{AW} = 80°$

For $\beta_{AW} = 80°$ shown in Fig. 3, two different trends can be observed for the evolution of drive force with sheet length. Depending on the panelling method, the curves show either one or two local maxima. The global maximum drive force is located on different trims regarding the verge of curling for the different spinnakers. The maximum drive force occurs before this limit for the triradial panelling contrary to the cross-cut one where a second local maximum is identified just after the verge of curling. In the AirX 500 case (Fig. 3b), the best performance is reached at the second local maximum, slightly eased after the verge of curling. In the SuperKote 0.75 case (Fig. 3d), drive force seems identical for the two maxima configurations, identified 100 mm before or slightly after the curling occurrence. At this tight AWA, no clear benefit of curling can be drawn.

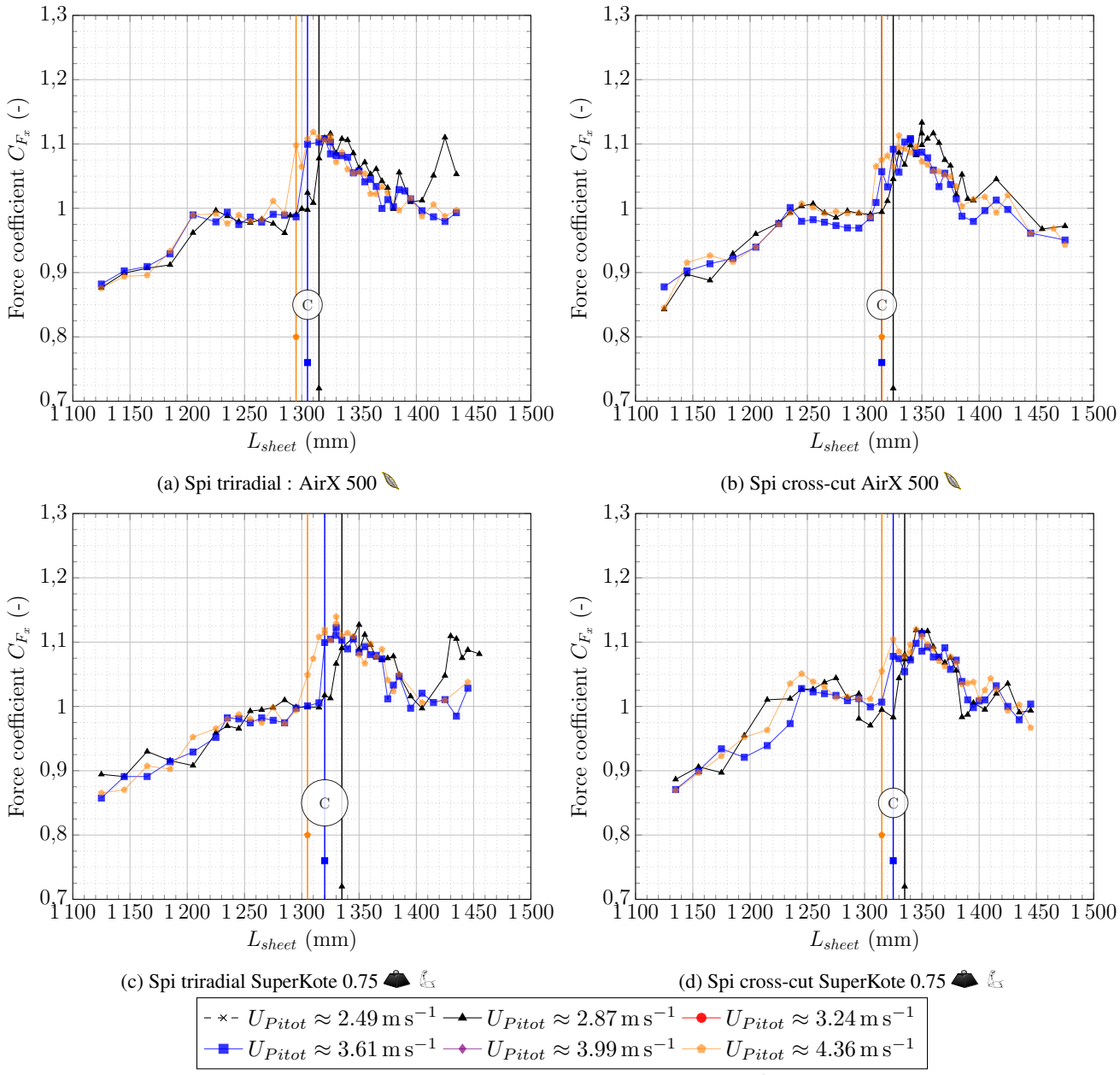

(a) Spi triradial : AirX 500

(b) Spi cross-cut AirX 500

(c) Spi triradial SuperKote 0.75

(d) Spi cross-cut SuperKote 0.75

Figure 5: Drive force coefficient C_{F_x} at $\beta_{AW} = 120°$. Vertical lines associated to Ⓒ represent the verge of curling for each flow velocity tested.

3.1.2 $\beta_{AW} = 100°$

For $\beta_{AW} = 100°$ a characteristic trend can be observed in Fig. 4 for the different spinnakers. After a smooth slope followed by a 50 mm plateau, a significant increase of the drive force occurs 10 mm to 20 mm around the verge of curling. The maximum is reached with a sheet eased 10 mm to 20 mm after this limit representing an increase up to 10% in the drive force compared to before curling.

When easing from this point, the drive force decreases as the curling area increases and is then replaced by a permanent fold for a greater sheet length. The aerodynamic performances of the spinnaker with a permanent fold are always deteriorated compared to the periodic curling state.

3.1.3 $\beta_{AW} = 120°$

For $\beta_{AW} = 120°$ shown in Fig. 5 the same trend than $\beta_{AW} = 100°$ can be described but with higher fluctuations in the driving force coefficient depending on the wind speed. At this AWA, the maximum is lower than at $\beta_{AW} = 100°$.

The driving force evolves significantly with the sheet length until reaching a maximum occuring after the verge of curling for the two larger AWA.

Standard deviation evolution of the drive force can also be significant between a non curling case and a curling case where it almost doubles for the two largest AWA as shown in Tab. 1. Such an observation could be used for curling detec-

tion thanks to the force signals with possible applications for autonomous onboard trimming system.

Standard deviation given in %						
β_{AW}	80°		100°		120°	
sail	nc	c	nc	c	nc	c
SPI TRI AirX 500	2	2.5	2.5	5	2.5	7
SPI TRI SuperKote 0.75	2	2.5	2.5	6	2.5	6.5
SPI CC SuperKote 0.75	1.75	2.5	1.5	4	3	6
SPI CC AirX 500	2	3	2.5	5	2.5	6.5

Table 1: Representative evolution of the standard deviation of the drive force C_{F_x}. nc stands for non curling case and c for curling case.

However, to understand the influence of the sheet length and the curling on the whole yacht balance, side force and sheet load should also be considered.

3.1.4 Curling effect on side force and sheet load coefficients

For the paper clarity, the side force and the sheet load are presented for only one spinnaker and one angle, the described trend being identical for all studied cases. Fig. 6 presents representative cases of the curling occurence effect on the side force and the sheet load coefficients. Curling does not affect significantly the mean side force coefficient once curling appears as illustrated in Fig. 6a. Curling seems however to slightly affect the slope of the side force coefficient curve where a small drop is observed after its occurrence, which could be beneficial.

The sheet load coefficient can be affected by the curling as illustrated in Fig. 6b where a local maximum is observed after the occurrence of curling. This local maximum is associated to the maximum drive force observed previously, aerodynamic forces being transmitted to the three points of the sail, thus the sheet. The higher the apparent wind angle, the more significant this local maximum in the sheet load coefficient. The curling effects on side force and sheet load coefficient remain significantly smaller than the ones observed on the drive force.

For the side force standard deviation given in Tab. 2, the evolution is smaller than the one for the drive force coefficient, except for the largest AWA.

Standard deviation given in %						
β_{AW}	80°		100°		120°	
sail	nc	c	nc	c	nc	c
SPI TRI AirX 500	1.5	2	2	3	2	6
SPI TRI SuperKote 0.75	1.5	2	2	3	2	6
SPI CC SuperKote 0.75	1.5	2	2	3	2.5	6
SPI CC AirX 500	1.75	2	2	3	2	6

Table 2: Representative evolution of the standard deviation of the side force C_{F_y}. nc stands for non curling case and c for curling case.

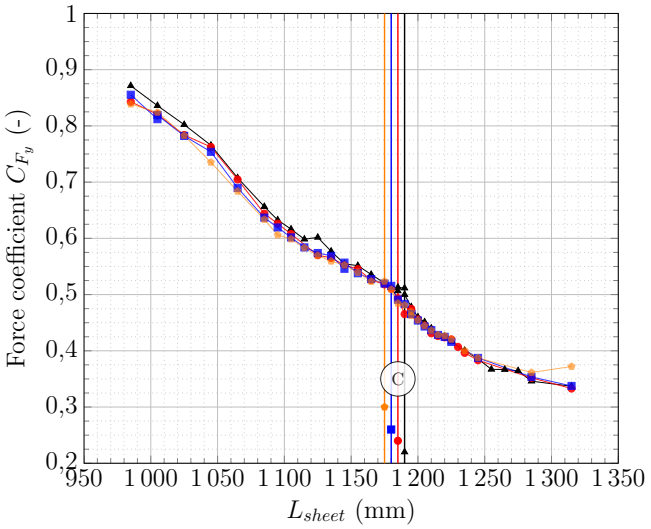

(a) Side force coefficient C_{F_y} for $\beta_{AW} = 100°$ for the spinnaker triradial SuperKote 0.75

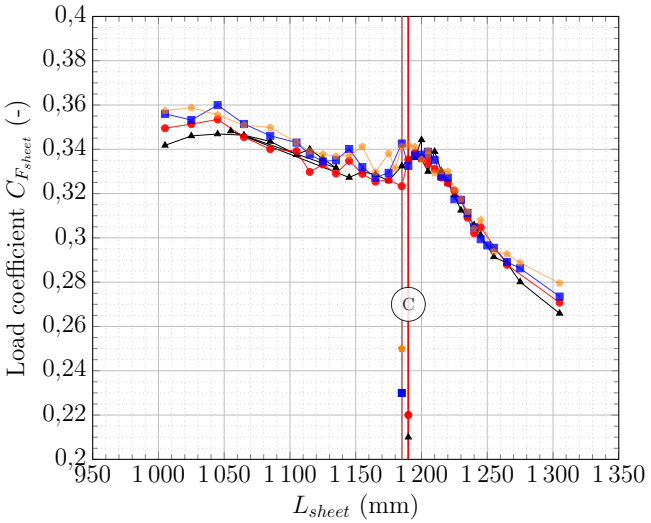

(b) Sheet load coefficient $C_{F_{sheet}}$ for $\beta_{AW} = 100°$ for the spinnaker crosscut AirX 500

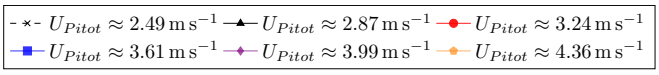

Figure 6: Side force and sheet load coefficient on representative cases. Vertical lines associated to Ⓒ represent the edge of curling for each flow velocity tested.

Differences between the four tested spinnakers are due to the panelling and cloths. Effect of the structural elements on the curling is detailed in the next paragraph.

3.1.5 Effect of panelling and materials on curling

For the different results obtained, we can observed that curling appears for a shorter sheet length for the triradial panelling. In the triradial panelling, the first top radial seam close to the front edge and nearly parallel to the luff (see Fig. 8a) seems to facilitate the folding process. On the contrary, the seam in the cross direction on the cross-cut sails (see in Fig. 8b) might increase the local luff stiffness

. Moreover the cross-cut panelling has equivalent or better performance than the triradial panelling, which is contrary to the common panelling choice in the J80 class where the triradial is massively preferred to cross-cut.

For a given panelling and flow speed, the lighter material AirX 500 triggers the curling for a shorter sheet length. The spinnaker being lighter, its flying shape tends to be more elevated with a top luff more likely to go on the windward side closer to the curling situation. Apart from $\beta_{AW} = 80°$, the faster the flow speed, the shorter the sheet length where curling appears, the sail being more likely to fly higher and closer to the curling situation.

3.2 RECOMMENDATIONS FOR SAILORS

Conclusions on the best practices regarding the curl of the spinnaker depend on the wind angle. Moreover, even if the results indicate that the verge of curling trim does not correspond directly to the optimal trim, i.e. the maximum mean drive force, it can still be used as an indicator.

Following the results observed in the wind tunnel :

- for $\beta_{AW} = 80°$ associated to situation close to reaching, the best driving force is obtained with a sail trimmed tighter than the curling occurrence for the triradial design and on the verge of curling for the cross-cut design.
- for $\beta_{AW} = 100°$ and $\beta_{AW} = 120°$, the sheet should be eased slightly after the curling occurrence and the sailor should let the spinnaker curl, as an overtrimmed spinnaker has a more detrimental effect on the driving force than an overeased one.

The best trim can provide up to 10% more mean drive force compared to the value measured on the plateau part occurring before the verge of curling. However the optimal trim peak width remains small representing about $23\,\mathrm{cm}$ sheet length amplitude at full-scale. In all cases measured, if the fold is maintained when the sail is largely eased, the driving force decreases and is no longer optimal.

3.3 TIME SERIES STUDIES

The presented results indicate that curling can have a significant effect on the averaged value of force coefficient. In order to better understand the curling effect, some analysis are carried out on time series in order to provide different information about the dynamic behaviour of this phenomenon.

One of the parameter of interest is the natural frequency of curling f_c which can be measured using time stamped photographs recorded by the triggered cameras. From this natural curling frequency, a dimensionless natural reduced curling frequency f_{rc} is defined like in [7] as:

$$f_{rc} = f_c \frac{\sqrt{S}}{U_{Pitot}} \tag{2}$$

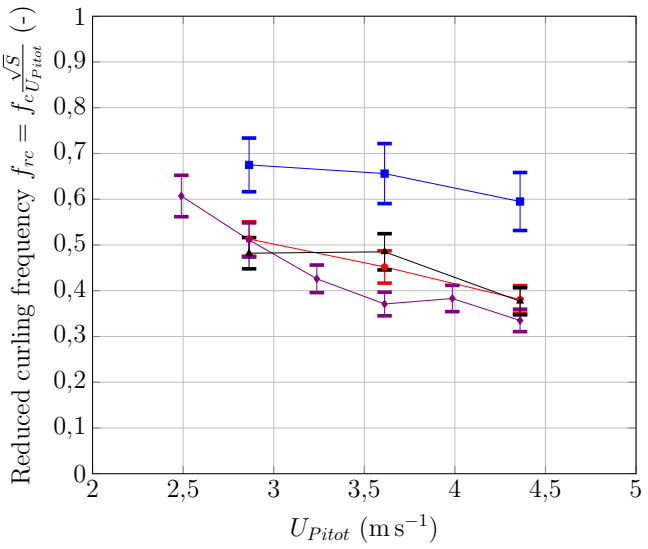

(a) $\beta_{AW} = 80°$

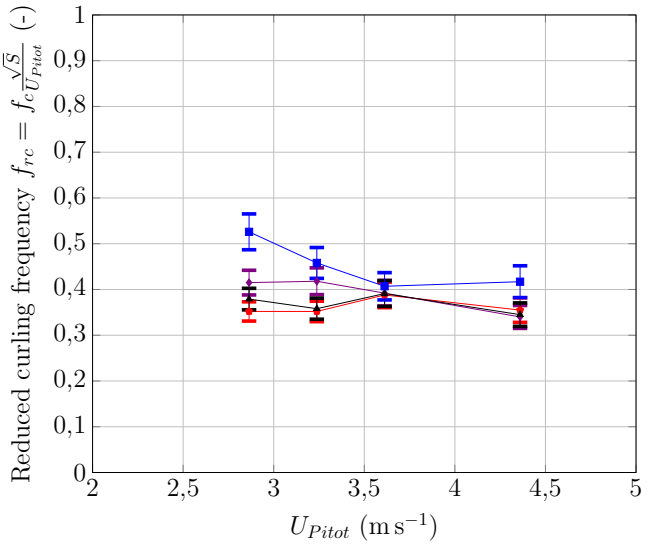

(b) $\beta_{AW} = 100°$

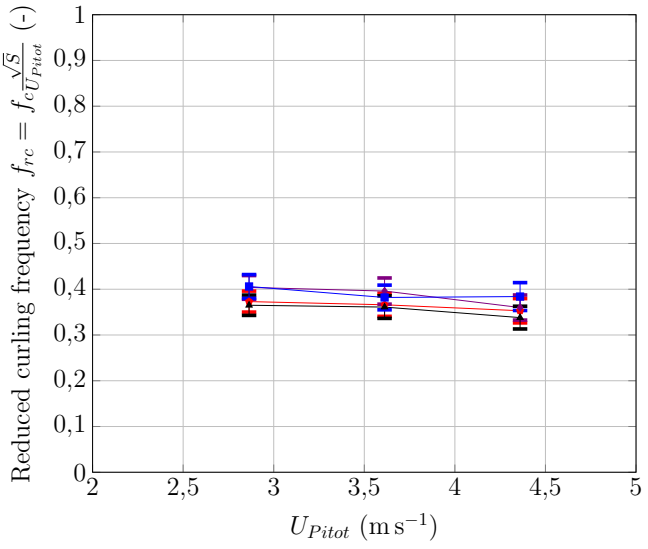

(c) $\beta_{AW} = 120°$

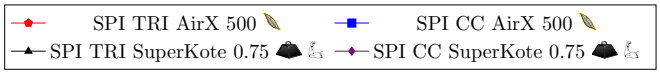

Figure 7: Reduced natural curling frequency evolution with the flow velocity. Error bars represent the uncertainty due to the frame rate of the recording camera device.

Fig. 7 gives the different natural reduced frequency of curling obtained by post processing of the time stamped photographs. The curling frequency can be extracted using different methods like usual power spectral density decomposition which reveals a peak at the expected frequency. Force signal processing allows to identify the frequency of curling more rapidly than manual visual post processing but needs more development to be extended to all measurements.

Depending of the apparent wind angle value, the results can either be structurally dependant at $\beta_{AW} = 80°$, slightly structurally dependant at $\beta_{AW} = 100°$ or fairly identical for the different spinnaker tested for $\beta_{AW} = 120°$ where the reduced natural curling frequency is close to 0.35 to 0.4. It means that especially in this last configuration, the curling frequency evolves linearly with the flow speed.

This identified curling frequency at $\beta_{AW} = 120°$, that can also be observed at $\beta_{AW} = 100°$, can be related to some fluid pattern frequencies observed in past studies like in [4, 5] where a Strouhal number associated to the reduced frequency of the pressure fluctuations measured at mid height of a rigid spinnaker is defined. The equivalent Strouhal value based here on the reference length $\sqrt{S}$ is about 0.12-0.36 where the higher range could correspond to the one identified for the curling dynamic shown here. Moreover in these studies, stronger fluctuations of pressure coefficient are observed after the mid-chord confirming these fluctuations are associated with a *"large scale vortex shedding in the flow separation"*. The global motion observed on the spinnaker, especially at $\beta_{AW} = 120°$, might suggest a lock in phenomenon between the curling phenomenon and the vortex induced motion driven by a more global phenomenon pattern such as a transient detachment flow identified in [4, 5]. Complementary transient flow information around an extruded 2D cambered plate, either experimental in [3] or numerical in [15], could be also compared to the identified reduced frequency presented here.

The measurement of the curling frequency is important as it could be used as a parameter which quantify the dynamic evolution aspect of the phenomenon. Such parameter could be used to validate phenomenological model of curling or the ability of unsteady fluid-structure interaction simulation to model the curling instability.

4 CONCLUSIONS

Curling effect is studied in wind tunnel for different spinnakers combining two different sail materials and panelling methods at different wind angles and velocities conditions. At $\beta_{AW} = 100°$ and $\beta_{AW} = 120°$, a significant effect is measured where curling increases up to 10% the mean driving force and doubles its standard deviation. Driven by the results, recommendation for sailors at these AWAs would be to ease the sheet after curling occurrence to obtain the best aerodynamic performance. Moreover, an overtrimmed spinnaker has a terrible impact on the driving force. Smaller effects are observed on side force and sheet load coefficients. Materials stiffness and panelling have an impact on the trimming where the sail starts to curl. Light material and tri-radial panelling spinnakers tend to curl with a shorter sheet length. At $\beta_{AW} \geq 100°$, curling frequency increases linearly with the wind speed and the calculated reduced frequency remains close to 0.4.

More investigations are carried out to define another relevant dimensionless parameter adapted to the curling dynamic, either based on local chord definition requiring further flying shape post processing, or focusing on the folding dynamic itself. Differences have been observed between wind tunnel and full-scale measurements provided by [7]. The temporal evolution of the aerodynamic forces according to the flying shape stage are different but in both studies, the curling phenomenon increases the dynamic evolution of loads and forces, generating higher loads and forces during the curling cycle compared to an overtrimmed non curling case. Wind tunnel can decouple the wind angle and wind speed effect compared to imposed full-scale sailing conditions. No flow investigation was carried out when curling occurs however it is reasonable to assume that such a behaviour is associated to a given flow phenomenon. Comparison with bluff body wake such as [3] and ribbon structure behaviour studies are under investigation but will need to be confirmed with measurements on soft sail. Flying shape post processing results not presented in this article are currently used for numerical simulations.

Many extensions of this work can be suggested. Here only static trim has been presented but a relevant extension of this work could study the effect of dynamic trimming like in [2] but on downwind sails modelling the trimmer action controlling the sail in an unsteady sailing environment. This investigation would be relevant especially for trimming frequency close to the natural curling frequency. The effect of heel, twisted flow and mainsail can also be investigated.

5 ACKNOWLEDGEMENTS

The authors are grateful to Incidence Sails. This work was supported by Brest Métropole Océane, the French Naval academy and has received fundings from the European Union's Seventh Programme for research, technological development and demonstration under grant agreement n°PIRSES-GA-2012-318924 (SAILING FLUIDS) and from the Royal Society of New Zealand, from the "Laboratoire d'Excellence" LabexMER (ANR-10-LABX-19) and co-funded by a grant from the French government under the program "Investissements d'Avenir", and from the European Union's Seventh Framework Programme (FP7/2007-2013) under REA grant agreement n°PCOFUND-GA-2013-609102 (PRESTIGE-Campus France).

REFERENCES

[1] A. Arredondo and I. M. Viola. On the leading edge vortex of thin wings. In *69th Annual meeting of the APS Division of Fluid Dynamics Meeting Abstracts*, volume 61, Portland, Oregon, USA, 2016.

[2] N. Aubin, B. Augier, P. Bot, F. Hauville, M. Sacher, and R. G. J. Flay. Wind tunnel investigation of dynamic trimming on upwind sail aerodynamics. In *The 22nd Chesapeake sailing yacht symposium*, pages 111–121, Annapolis, Maryland, USA, 2016.

[3] P. Bot, M. Rabaud, G. Thomas, A. Lombardi, and C. Lebret. Sharp transition in the lift force of a fluid flowing past nonsymmetrical obstacles: Evidence for a lift crisis in the drag crisis regime. *Physical Review Letters*, 117(23), 2016.

[4] P. Bot, I. M. Viola, R. G. J. Flay, and J.-s. Brett. Wind-Tunnel pressure measurements on model-scale semi-rigid downwind sails. In *The Third International Conference on Innovation in High Performance Sailing Yachts (Innovsail)*, pages 119–127, Lorient, France, 2013.

[5] P. Bot, I. M. Viola, R. G. J. Flay, and J.-S. Brett. Wind-tunnel pressure measurements on model-scale rigid downwind sails. *Ocean Engineering*, 90:84–92, 2014.

[6] I. M. C. Campbell. A comparison of downwind sail coefficients from tests in different wind tunnels. *Ocean Engineering*, 90:62–71, 2014.

[7] J. Deparday. *Experimental studies of Fluid-Structure Interaction on Downwind Sails*. PhD thesis, Université de Bretagne Occidentale, Brest, 2016.

[8] M. Durand, F. Hauville, P. Bot, B. Augier, Y. Roux, A. Leroyer, and M. Visonneau. Unsteady numerical simulations of downwind sails. In *International Conference on Innovation in High Performance Sailing Yachts*, Lorient, France, 2010.

[9] M. Durand. *Interaction fluide-structure souple et légère, applications aux voiliers*. PhD thesis, Ecole Centrale de Nantes, 2012.

[10] M. Durand, A. Leroyer, C. Lothodé, F. Hauville, M. Visonneau, R. Floch, and L. Guillaume. FSI investigation on stability of downwind sails with an automatic dynamic trimming. *Ocean Engineering*, 90:129–139, 2014.

[11] R. G. J. Flay. A twisted flow wind tunnel for testing yacht sails. *Journal of Wind Engineering and Industrial Aerodynamics*, 63(1-3):171–182, 1996.

[12] M. Lombardi, M. Cremonesi, A. Giampieri, N. Parolini, and A. Quarteroni. A strongly coupled fluid-structure interaction model for wind-sail simulation. In *4th High Performance Yacht Design*, pages 212–221, Auckland, New Zealand, 2012.

[13] D. Motta. *An experimental investigation of full-scale sail aerodynamics using pressures, shapes and forces*. PhD thesis, The University of Auckland, 2015.

[14] D. Motta, R. G. J. Flay, P. J. Richards, D. J. Le Pelley, J. Deparday, and P. Bot. Experimental investigation of asymmetric spinnaker aerodynamics using pressure and sail shape measurements. *Ocean Engineering*, 90:104–118, 2014.

[15] S. Nava, P. Bot, J. Cater, and S. Norris. Modelling the lift crisis of a cambered plate at 0° angle of attack. In *20th Australasian Fluid Mechanics Conference*, Perth, Australia, 2016.

[16] H. Renzsch and K. Graf. Fluid-structure interaction simulation of spinnakers - getting close to reality. In *The Second International Conference on Innovation in High Performance Sailing Yachts*, Lorient, France, 2010. Royal Institution of Naval Architects.

[17] H. Renzsch and K. Graf. An experimental validation case for fluid-structure-interaction simulations of downwind sails. In *The 21st Chesapeake Sailing Yacht Symposium*, Annapolis, Maryland, USA, 2013.

[18] D. Trimarchi, M. Vidrascu, D. Taunton, S. Turnock, and D. Chapelle. Wrinkle development analysis in thin sail-like structures using MITC shell finite elements. *Finite Elements in Analysis and Design*, 64:48–64, 2013.

[19] I. M. Viola. Downwind sail aerodynamics: A CFD investigation with high grid resolution. *Ocean Engineering*, 36(12):974–984, 2009.

[20] I. M. Viola, S. Bartesaghi, T. Van-Renterghem, and R. Ponzini. Detached Eddy Simulation of a sailing yacht. *Ocean Engineering*, 90:93–103, 2014.

[21] I. M. Viola and R. G. J. Flay. Force and Pressure Investigation of Modern Asymmetric Spinnakers. *International Journal of Small Craft Technologie*, 151, 2009.

[22] I. M. Viola and R. G. J. Flay. Sail pressures from full-scale, wind-tunnel and numerical investigations. *Ocean Engineering*, 38(16):1733–1743, 2011.

[23] I. M. Viola and R. G. J. Flay. Pressure distributions on modern asymmetric spinnakers. *International Journal of Small Craft Technology*, 152(1):41–48, 2015.

[24] I. M. Viola and R. E. Muir. The leading-edge vortex of swift wings. *bioRxiv, the preprint server for biology*, (https://doi.org/10.1101/099713), 2017.

6 AUTHORS BIOGRAPHY

N. Aubin, PhD. His previous experience includes fluid-structure interaction research on yacht sails, especially on unsteady situations (mainsail pumping and spinnaker curling). He achieved his master thesis studying fleet interferences using the Twisted Flow Wind Tunnel of the Yacht

Research Unit of the University of Auckland. He obtained his master of engineering and master of applied mechanics in hydrodynamics and ocean engineering from Ecole Centrale de Nantes in 2013.

B. Augier, PhD holds the current position of associate researcher at the Naval Academy Research Institute-IRENav. He is involved since 2008 in the VoileNav project which concerns activities in the field of fluid dynamics applied to sailing yachts. His current research interest includes, both by numerical and experimental approaches, problems of fluid structure interaction applied to yacht sails and hydrofoils in composite materials. His previous experience includes the development of an dedicated instrumentation for full-scale yacht tests and hydrodynamic propulsion system.

J. Deparday holds a PhD in fluid-structure interaction from the Naval Academy Research Institute. He developed and improved an instrumented J/80 to measure loads, pressures and sail shapes resolved in time. Previously he worked during 2 years in the Netherlands as a Naval Architect, and obtained his Master of Science in Engineering from ENSTA-Bretagne in Brest in 2010. He carried out his master thesis at the Yacht Research Unit-Kiel.

M. Sacher holds the current position of PhD student in sailing yacht performance optimization at the Naval Academy Research Institute. Previously he worked during 1 year at the Newcastle University in computational fluid dynamics, and obtained his dual Engineer degree from ESTACA in aviation and Master of Science in Naval Environment from ENSAM - French Naval Academy in 2014. He carried out his master thesis at the K-Epsilon company.

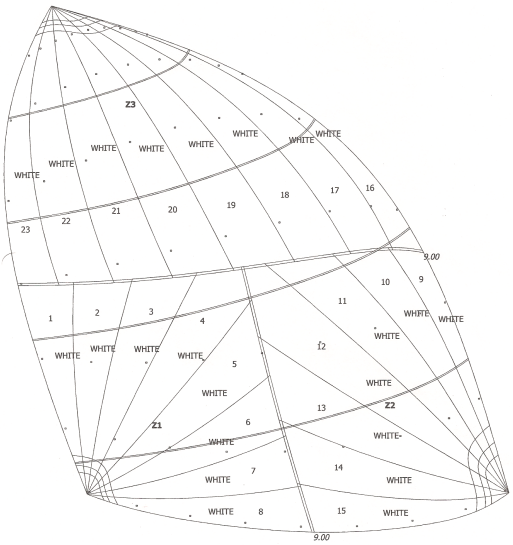

(a) Illustration of triradial panelling

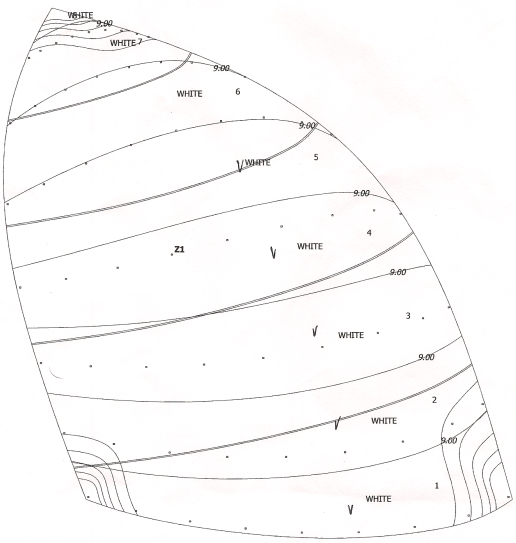

(b) Illustration of cross-cut panelling

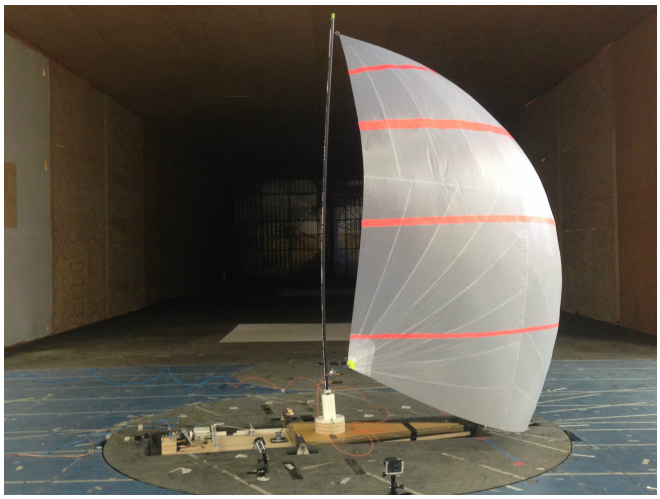

(c) Triradial manufactured in 2015: AirX 500

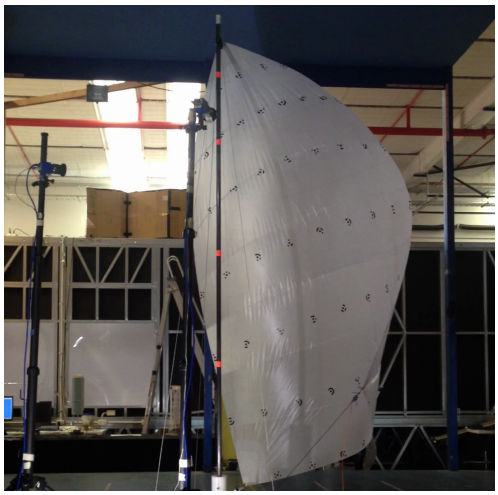

(d) Cross-cut manufactured in 2016: AirX 500

(e) Triradial manufactured in 2016: SuperKote 0.75

(f) Cross-cut manufactured in 2015: SuperKote 0.75

Figure 8: Model spinnakers photographs. The results presented in this paper correspond to a full rig cantilevered mast as shown on Figs. 8e and 8e. Each column represent one type of panelling and each line represents one material.